EUROFUSION WP15ER-PR(16) 16059

F Nespoli et al.

Blob properties in nonlinear simulations of the TCV Scrape-Off Layer

Preprint of Paper to be submitted for publication in
22nd International Conference on Plasma Surface Interactions
in Controlled Fusion Devices (22nd PSI)

This work has been carried out within the framework of the EUROfusion Consortium and has received funding from the Euratom research and training programme 2014-2018 under grant agreement No 633053. The views and opinions expressed herein do not necessarily reflect those of the European Commission.

Nonlinear simulations of the TCV Scrape-Off Layer

F. Nespoli, B. Labit, I. Furno, F.D. Halpern, P. Ricci, F. Riva
Ecole Polytechnique Fédérale de Lausanne (EPFL), Swiss Plasma Center (SPC), CH-1015 Lausanne, Switzerland

Abstract

To investigate the mechanisms leading to the heat deposition on the first wall in the Scrape Off-Layer (SOL), we perform dedicated numerical nonlinear simulations of the SOL plasma dynamics of a TCV discharge using the GBS code [1, 2]. The simulated parallel heat flux profiles on the limiter agree qualitatively with the experimental ones obtained by means of infrared thermography [3], showing a double scale length. Non-ambipolar currents are found to flow to the limiter, consistenlty with the experiments. The contribution of the latters to the total heat flux is discussed. The results of a second simulation identical to the first one but with 40 times higher resistivity are also discussed.

---

1 Introduction

Inboard limited L-mode discharges are foreseen in ITER for the start-up and ramp-down phases resulting in large heat fluxes deposited from the plasma onto the first wall [4]. Dedicated experiments were performed in TCV [3] and other tokamaks to measure such heat fluxes. Two distinct regions in the Scrape-Off Layer (SOL) were observed. The near SOL, extending a few millimeters from the last closed flux surface (LCFS), is characterized by a steep gradient of the parallel heat flux and is of crucial importance for the first wall peak heat loads. The far SOL, characterized by flatter profiles, is typically a few centimeters wide and is at the origin of the main heat loss channel onto the first wall. Following these findings, the design of the ITER first wall panels was changed to sustain a larger heat flux due to the near SOL [5]. Still, the physics determining the double scale length in the SOL is not yet fully understood.

2 Non linear simulations with the GBS code

To better understand the mechanisms leading to the heat deposition on the first wall, we perform dedicated numerical nonlinear simulations of the SOL plasma dynamics using the GBS code [1]. By solving the drift-reduced Braginskii equations, GBS allows for the self-consistent description of equilibrium and fluctuating quantities in a fully 3D geometry. Finite aspect ratio effects, ion temperature and magnetic shear are included in the simulations. The equations determining the plasma dynamics and the boundary conditions are exposed in detail in ref.[2] and [6], respectively. These simulations feature open field lines and the LCFS is set by the position of the plasma density and temperature source that mimics the injection of plasma from the core. The position and amplitude of the sources could hence affect quantitatively the results. Simulations including both open and closed field line regions are ongoing, whose first results have been presented in [7], to better address the physics at the LCFS and in the near SOL.

In this paper the results of two simulations are discussed: in the first one (A), the SOL of a TCV discharge is modeled. This is a circular inboard limited ohmic L-mode plasma. The values of the plasma density and temperature at the LCFS, $n_{e,LCFS} = 5 \times 10^{18}$ m^{-3} and $T_{e,LCFS} = 25$ eV, are deduced from Langmuir Probes embedded in the limiter. They set the normalized Spitzer resistivity $\nu = en_{e,LCFS}R_0/(m_i c_{s,LCFS}\sigma_\parallel) \propto n_{e,LCFS}R_0\lambda/(m_i/m_e c_{s,LCFS}T^{3/2}_{e,LCFS})$ and the

adimensionalized size of the system through the ion sound Larmor radius ρ_s. The safety factor $q = 3.2$, the magnetic shear $\hat{s} = 1.5$ and the aspect ratio are consistent with the magnetic reconstruction of the discharge. The ion temperature at the LCFS is assumed to be $T_{i,LCFS} = T_{e,LCFS}$. In this simulation, the toroidal field and the plasma current are antiparallel, while in the experiment they are parallel. This could lead to some discrepancies when comparing numerical and experimental results. A snapshot of the density of simulation A is shown in Fig. 1 together with the limiter geometry for the simulation (red) and TCV (dashed black) respectively. The main simulation parameters are displayed. The second simulation (B) is identical to the first one, exception made for the resistivity, that is 40 times higher. This choice is driven by the trend exposed in [3], i.e. that the heat flux associated with the near SOL increases with electron temperature and decreases with plasma density $\Delta P_{SOL} \propto T_e^{1.5} n_e^{-1} \propto \nu$.

3 Comparison with the experimental data

The numerical simulations provide the temporal evolution in 3D of the plasma density n (quasi neutrality is assumed), the electron and ion temperature T_e and T_i, the electron and ion parallel velocities $v_{||,e}$ and $v_{||,i}$. The equilibrium 2D profiles are obtained averaging over time and the toroidal direction. The plasma pressure and parallel current are computed as $p = n(T_e + T_i)$ and $j_{||} = en(v_{||,i} - v_{||,e})$ respectively. The parallel heat fluxes arriving on the limiters are $q_{||} = q_{||,e} + q_{||,i}$, with $q_{||,e} = \frac{5}{2} n T_e v_{||,e} - 0.71 \frac{j_{||}}{e} T_e$ and $q_{||,i} = \frac{5}{2} n T_i v_{||,i} + n v_{||,i}^3$.
The term including the kinetic energy of the net ion flow is often referred to as macroscopic heat flux. The term including the paralle current comes from the Braginskii closure of the energy equation and is referred to as microscopic heat flux. Similarly, the terms proportional to ion and electron temperature are called mesoscopic heat fluxes, happening on a scale in between the macroscopic and the microscopic ones. The simulated parallel heat flux radial profiles on the limiter are well described by a sum of two exponentials $q_{||} = q_s \exp(-r_u/\lambda_s) + q_l \exp(-r_u/\lambda_l)$ where r_u is the upstream coordinate (being $r_u = 0$ at the LCFS). The resulting values for simulation A of $\lambda_s = 2.9,\ 2.8$ mm and $\lambda_l = 37,\ 39$ mm for the upper and lower limiter respectively agree quantitatively with the experimental ones obtained by means of infrared thermography $\lambda_{s,IR} = 3.2$ mm, $\lambda_{l,IR} = 37$ mm (the infrared analysis was possible only for the upper part of the limiter), as shown in Fig.2. Though, the relative importance of the near SOL is much smaller, being $q_s/q_l \sim 0.5$ in the simulation and $q_s/q_l \sim 5$ in the experiment. Also, the values of λ_l are in good agreement with the theoretical prediction for the main SOL from ref.[8], giving $\lambda_q = 33$ mm.
A double scale length is observed in the pressure radial profiles as well; the pressure radial profiles fit well to a sum of two exponentials $p = p_s \exp(-r_u/\lambda_s) + p_l \exp(-r_u/\lambda_l)$. The poloidal variation of the two scale lengths is shown in Fig.3, color coded with the relative strength of the near SOL p_s/p_l.
Also, net electron currents flow to the limiter in the near SOL, as it is observed experimentally with Langmuir probes, confirming their importance in the formation of the narrow feature. The comparison between simulated and measured currents is shown in fig.4. The difference in behavior of such currents in the far SOL between the simulation and the experiment is under investigation and it is probably due to the Boussinesq approximation [9] and the boundary conditions. In Fig.5 the microscopic heat flux associated with the non-ambipolar current is compared with the mesoscopic and microscopic ones. As a result, its contribution to the total heat flux is negligible. This confirms what already suggested in ref. [10], that even though non-ambipolar currents are strictly related to the presence of a steep-gradient near SOL, they are not responsible for the excess heat flux arriving to the limiter.
In simulation B, as the resistivity is increased by 40 times, the heat flux profiles at the limiters still fit well to a sum of two exponentials. Though,

the increase of the resistivity causes the SOL to flatten and the poloidal asymmetry to increase: $\lambda_s = 5.7,\ 3.5$ mm, $\lambda_l = 110,\ 59$ mm for the upper and lower limiter respectively. The widening of the far SOL and the increase of the poloidal asymmetry is observed in the pressure profiles as well, as shown in Fig.3. The importance of the short scale length remains strong close to the limiters, but it tends to vanish on the low field side. The widening of the SOL is due to an overall reduction of the $\mathbf{E}\times\mathbf{B}$ velocity flow, as shown in Fig.6, where the poloidal average of $v_{EXB,\theta}$ is displayed for the two cases. In both simulations the $\mathbf{E}\times\mathbf{B}$ flow is mainly poloidal towards the upper limiter, its radial component being negligible.

As the resistivity is increased in simulation B, the current flowing to the upper limiter is reduced by a factor 2, while the one flowing to the lower limiter does not vary substantially.

The poloidally averaged skewness profiles for density fluctuations are shown in Fig.7 for the two simulations. The skewness increases moving away from the LCFS, being > 0.5 in the far SOL. Also, as the resistivity is increased, the skewness almost doubles. The positive skewness is an indication of the presence of blobs, that can play an important role in the transport in the far SOL. The dynamics of the blobs and their impact on heat transport in the SOL will be discussed in a future work.

4 Conclusions

A first dedicated nonlinear numerical simulation of the TCV SOL is presented. The heat fluxes arriving to the limiter agree well with the experimental data from IR thermography, showing the presence of two distinct regions in the SOL. Also, non-ambipolar electron currents flowing to the limiters are observed, qualitatively agreeing with the experiments. This confirms the correlation between non-ambipolar currents and the formation of a double scale length in the SOL. Though, the heat flux associated with such currents does not contribute substantially to the total heat flux deposited on the limiter.

The increase of resistivity by a factor of 40 causes the suppression of the poloidal $\mathbf{E}\times\mathbf{B}$ velocity, resulting in an overall wider main SOL. The presence of a double scale length remains strong at the limiters, while it tends to disappear on the low field side. To give a better insight of the physics in the near SOL, the application of the same analysis to ongoing simulations including both open and closed field line regions is foreseen.

Acknowledgments

This work has been carried out within the framework of the EUROfusion Consortium and has received funding from the Euratom research and training programme 2014-2018 under grant agreement No 633053. The views and opinions expressed herein do not necessarily reflect those of the European Commission.

References

[1] P. Ricci et al., Plasma Phys. Controlled Fusion 54 (2012) 124047

[2] F. D. Halpern, et al., J. Comput. Phys. 315 (2016) 388-408

[3] F. Nespoli, et al., J. Nucl. Mater. 463 (2015) 393-396

[4] R.A. Pitts et al., J. Nucl. Mater. 415 (2011) 957-964

[5] M. Kocan, et al., Nucl. Fusion 55 (2015) 033019

[6] J. Loizu, et al., Phys. of Plasmas 19 (2012) 122307

[7] F. D. Halpern, 57th Annual Meeting of the APS DPP, Nov. 16-20, 2015, Savannah (GA)

[8] F. D. Halpern et al., Nucl. Fusion 53 (2013)

[9] J. Loizu, private communication

[10] R.Dejarnac et al., J. Nucl. Mater. 463 (2015) 381-384

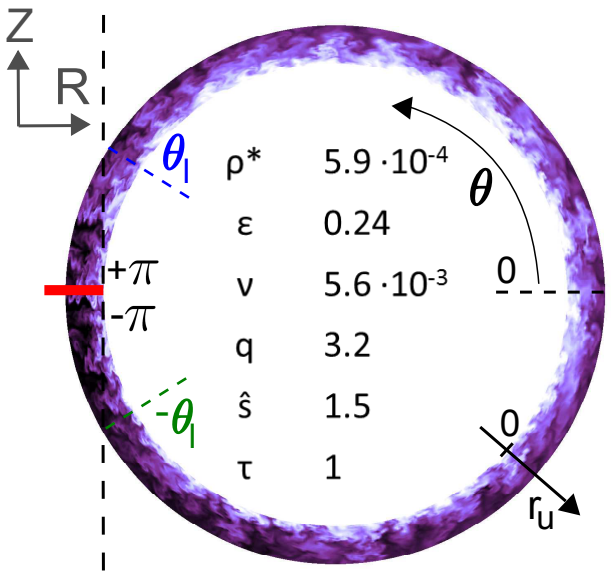

Figure 1: Snapshot of the density from simulation A. The coordinate system is displayed together with the simulation (thick red) and TCV (dashed black) limiter geometry. The $q_{||}$ and $j_{||}$ profiles on the limiters are computed as poloidal averages for $\theta_l \leq \theta \leq \pi$ (top) and $-\pi \leq \theta \leq -\theta_l$ (bottom). The simulation parameters are displayed: $\rho^* = \rho_s/R$, the aspect ratio ϵ, the normalized Spitzer resistivity ν, the safety factor q, the magnetic shear $\hat{s}$ and $\tau = T_{i,LCFS}/T_{e,LCFS}$.

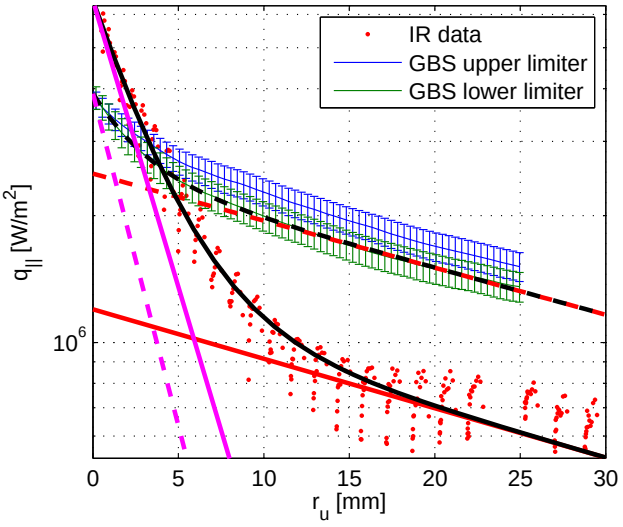

Figure 2: Heat flux onto the upper and lower limiters (blue and green respectively) compared with experimental data from IR thermography (red dots) . The flux is poloidally averaged over the extent of the real geometry of the TCV limiter, displayed in fig.1. The fit with the sum of two exponentials is shown (black lines), the short exponential in magenta and the long one in red, continuous lines for experimental data and dashed for one of the two limiters in the simulation. The simulated slopes of far and near SOL match the ones from experiment, not the magnitude of the associated heat fluxes.

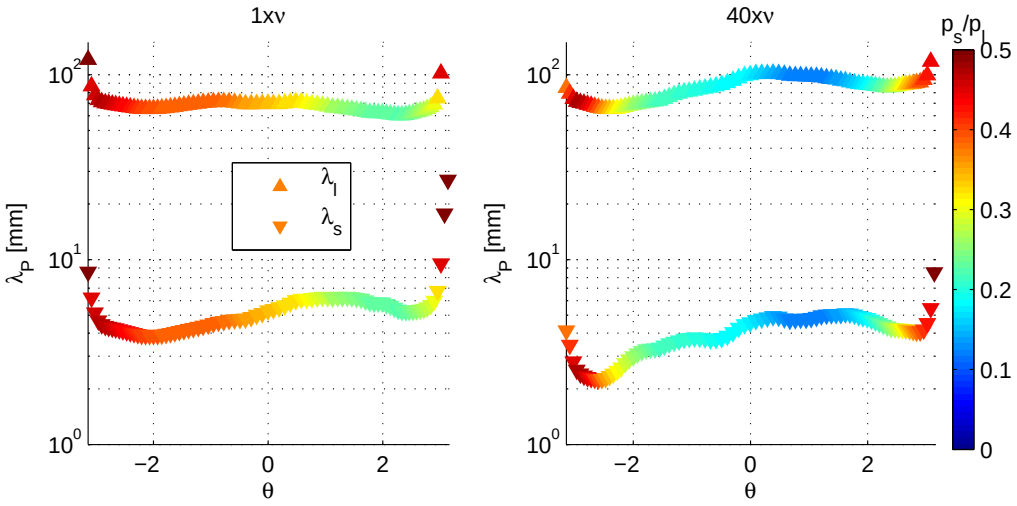

Figure 3: Poloidal variation of the two decay lengths resulting from the fit of the pressure profiles with the sum of two exponentials, color coded with the relative strength of the short component. Simulation A on the left, simulation B on the right. The increase of resistivity causes the near SOL to become relatively less important on the low field side.

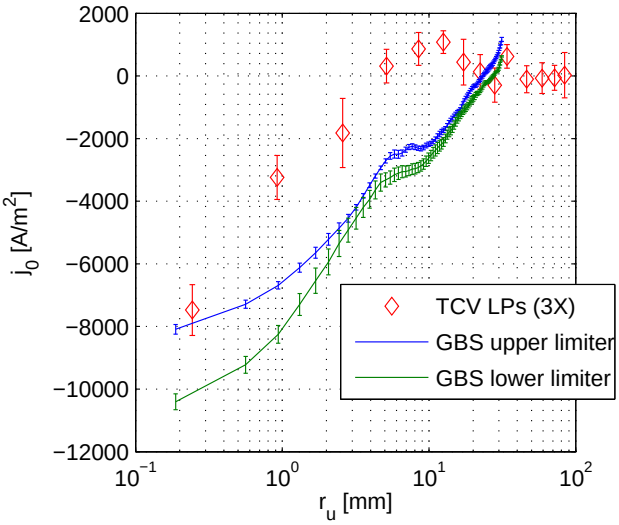

Figure 4: The parallel currents arriving to the limiters in the GBS simulations (blue and green). They qualitatively with the current density arriving to the grounded wall measured in TCV using flush mounted Langmuir probes (red diamonds, rescaled for plotting).

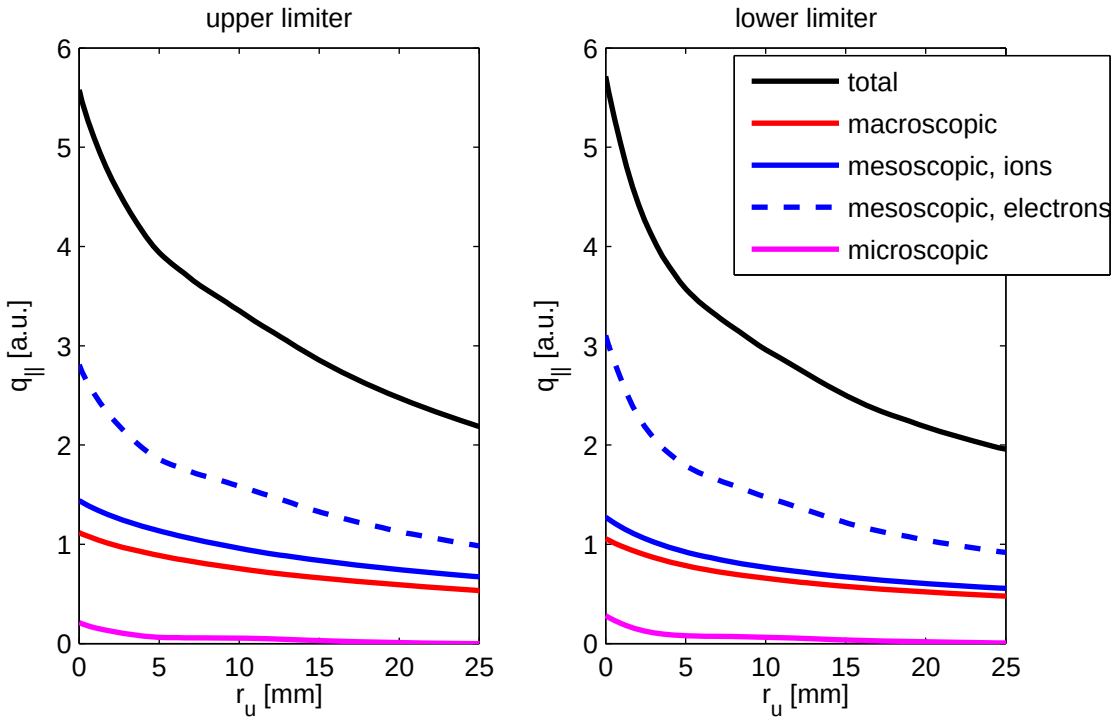

Figure 5: Different components contributing to the heat flux arriving onto the upper and lower limiters. The microscopic heat flux associated to the non ambipolar currents contributes only marginally to the total heat flux.

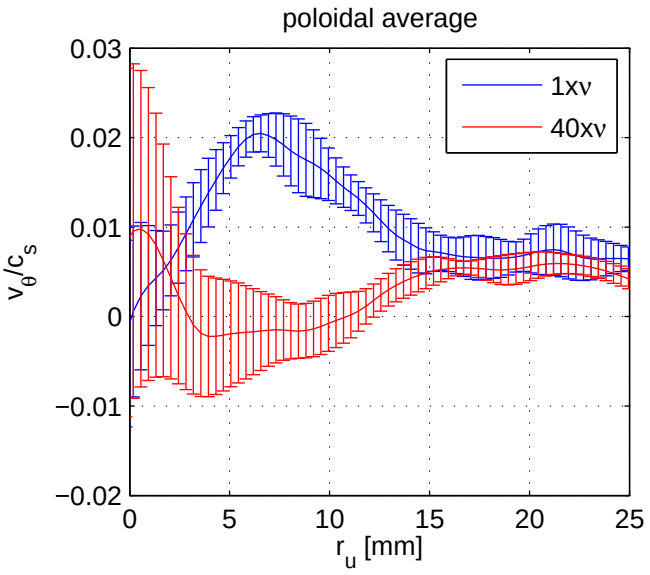

Figure 6: Poloidal average of the poloidal component of the $\mathbf{E} \times \mathbf{B}$ flow for simulation A (blue) and B (red). As the resistivity is increased, the poloidal flow is suppressed resulting in a wider far SOL.

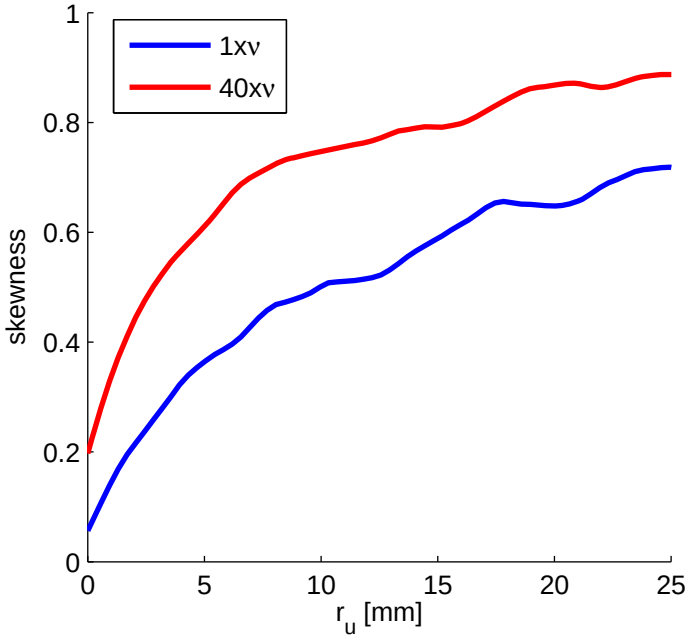

Figure 7: Poloidal average of the skewness of the density fluctuations for simulation A (blue) and B (red). The skewness increases moving away from the LCFS . The skewnees for simulation B is almost a factor 2 higher than in simulation A.